Plasmonic amplification for bioassays with epi-fluorescence readout

Martin Bauch, Simone Hageneder and Jakub Dostalek*

AIT - Austrian Institute of Technology, Biosensor Technologies, Muthgasse 11, 1190 Vienna, Austria
jakub.dostalek@ait.ac.at

Abstract: Corrugated metallic surfaces offer means for efficient amplification of fluorescence bioassay signal based on the near field coupling between surface plasmons and fluorophore emitters that are used as labels. This paper discusses the design of such plasmonic structure to enhance the sensitivity of immunoassays with epi-fluorescence readout geometry. In particular, crossed gold grating is theoretically and experimentally investigated for combined increasing of the excitation rate at the fluorophore excitation wavelength and utilizing directional surface plasmon-coupled fluorescence emission. For Alexa Fluor 647 dye, the enhancement factor of around $EF = 10^2$ was simulated and experimentally measured. When applied to a sandwich interleukin-6 immunoassay, highly surface-selective enhancement reaching a similar value was observed. Besides increasing the measured fluorescence signal associated with the molecular binding events on a surface by two orders of magnitude, the presented approach enables measuring kinetics of the surface reaction that is otherwise masked by strong background signal originating from bulk solution.

OCIS codes: (240.6680) Surface plasmons; (170.6280) Spectroscopy, fluorescence and luminescence; (280.1415) Biological sensing and sensors; (050.6624) Subwavelength structures; (170.2520) Fluorescence microscopy; (250.5403) Plasmonics.

References and links

1. W. H. Weber and C. F. Eagen, "Energy transfer from an excited dye molecule to the surface plasmons of an adjacent metal," Opt. Lett. **4**(8), 236–238 (1979).
2. G. W. Ford and W. H. Weber, "Electromagnetic interactions of molecules with metal surfaces," Phys. Rep. **113**(4), 195–287 (1984).
3. J. W. Attridge, P. B. Daniels, J. K. Deacon, G. A. Robinson, and G. P. Davidson, "Sensitivity enhancement of optical immunosensors by the use of a surface plasmon resonance fluoroimmunoassay," Biosens. Bioelectron. **6**(3), 201–214 (1991).
4. J. R. Lakowicz, J. Malicka, I. Gryczynski, and Z. Gryczynski, "Directional surface plasmon-coupled emission: A new method for high sensitivity detection," Biochem. Biophys. Res. Commun. **307**(3), 435–439 (2003).
5. J. S. Yuk, M. Trnavsky, C. McDonagh, and B. D. MacCraith, "Surface plasmon-coupled emission (SPCE)-based immunoassay using a novel paraboloid array biochip," Biosens. Bioelectron. **25**(6), 1344–1349 (2010).
6. W. Knoll, M. R. Philpott, and J. D. Swalen, "Emission of light from Ag metal gratings coated with dye monolayer assemblies," J. Chem. Phys. **75**(10), 4795–4799 (1981).
7. S. C. Kitson, W. L. Barnes, and J. R. Sambles, "Photoluminescence from dye molecules on silver gratings," Opt. Commun. **122**(4-6), 147–154 (1996).
8. T. Liebermann and W. Knoll, "Surface-plasmon field-enhanced fluorescence spectroscopy," Colloids Surf. A Physicochem. Eng. Asp. **171**(1-3), 115–130 (2000).
9. M. Bauch, K. Toma, M. Toma, Q. Zhang, and J. Dostalek, "Plasmon-enhanced fluorescence biosensors: a review," Plasmonics **9**(4), 781–799 (2014).
10. J. R. Lakowicz, K. Ray, M. Chowdhury, H. Szmacinski, Y. Fu, J. Zhang, and K. Nowaczyk, "Plasmon-controlled fluorescence: a new paradigm in fluorescence spectroscopy," Analyst (Lond.) **133**(10), 1308–1346 (2008).
11. J. Dostálek and W. Knoll, "Biosensors based on surface plasmon-enhanced fluorescence spectroscopy," Biointerphases **3**(3), FD12–FD22 (2008).

12. P. Holzmeister, G. P. Acuna, D. Grohmann, and P. Tinnefeld, "Breaking the concentration limit of optical single-molecule detection," Chem. Soc. Rev. **43**(4), 1014–1028 (2014).
13. K. Tawa, M. Umetsu, T. Hattori, and I. Kumagai, "Zinc oxide-coated plasmonic chip modified with a bispecific antibody for sensitive detection of a fluorescent labeled-antigen," Anal. Chem. **83**(15), 5944–5948 (2011).
14. X. Q. Cui, K. Tawa, K. Kintaka, and J. Nishii, "Enhanced fluorescence microscopic imaging by plasmonic nanostructures: from a 1D grating to a 2D nanohole array," Adv. Funct. Mater. **20**(6), 945–950 (2010).
15. K. Tawa, X. Q. Cui, K. Kintaka, J. Nishii, and K. Morigaki, "Sensitive bioimaging in microfluidic channels on the plasmonic substrate: Application of an enhanced fluorescence based on the reverse coupling mode," J. Photochem. Photobiol. Chem. **221**(2-3), 261–267 (2011).
16. Y. H. Tan, M. Liu, B. Nolting, J. G. Go, J. Gervay-Hague, and G.-Y. Liu, "A nanoengineering approach for investigation and regulation of protein immobilization," ACS Nano **2**(11), 2374–2384 (2008).
17. L. Chaiet and F. J. Wolf, "The properties of streptavidin, a biotin-binding protein produced by *Streptomycetes*," Arch. Biochem. Biophys. **106**, 1–5 (1964).
18. M. Toma, K. Toma, P. Adam, J. Homola, W. Knoll, and J. Dostálek, "Surface plasmon-coupled emission on plasmonic Bragg gratings," Opt. Express **20**(13), 14042–14053 (2012).
19. K. Toma, M. Vala, P. Adam, J. Homola, W. Knoll, and J. Dostálek, "Compact surface plasmon-enhanced fluorescence biochip," Opt. Express **21**(8), 10121–10132 (2013).
20. M. Bauch and J. Dostalek, "Collective localized surface plasmons for high performance fluorescence biosensing," Opt. Express **21**(17), 20470–20483 (2013).
21. P. B. Johnson and R. W. Christy, "Optical constants of noble metals," Phys. Rev. B **6**(12), 4370–4379 (1972).
22. P. Bharadwaj and L. Novotny, "Spectral dependence of single molecule fluorescence enhancement," Opt. Express **15**(21), 14266–14274 (2007).

1. Introduction

The emission of fluorophore emitters placed above a metallic surface was firstly investigated in 70-ties of the last century [1]. This study showed that the lifetime of the excited fluorophore is dramatically reduced due to the coupling with so called surface lossy waves (quenching due to dipole-dipole interactions with electrons occurs at distances below Förster radius of $f \sim 10$ nm) and propagating surface plasmons (that is observed at longer distances $f <$ 100 nm) [2]. The emitted photons that are trapped by propagating surface plasmon (PSP) modes can be partially recovered by reverse Kretschmann configuration [3–5] or by periodic corrugation of the metal surface [6, 7]. These techniques for out-coupling of PSPs allow extracting the emitted fluorescence photons from the surface to a highly directional fluorescence beam that can be delivered to a detector. The coupling of fluorophores with PSPs was exploited in fluorescence bioassays where fluorophore emitters are used as labels to report affinity binding of target molecules from an aqueous sample to the surface with attached recognition elements such as antibodies [3, 8]. The interaction of fluorophore labels with PSPs at their absorption λ_{ab} and emission λ_{em} wavelengths allows for increasing their "brightness" and thus offer means to detect smaller number of captured molecules on the surface. In analytical applications, this translates to the possibility of detecting trace amounts of analyte in a sample with improved limit of detection (LOD) [9–11]. In addition, the plasmonic amplification of fluorescence intensity allows increasing the signal-to-noise ratio in single molecule fluorescence spectroscopy that is expected to offer means for probing larger detection volumes and thus sensing of ultra-low concentration of molecules [12].

In general, the fluorescence signal from an emitter at a metallic surface can be plasmonically amplified by the combination of (locally) increased excitation rate by PSP-enhanced field intensity at λ_{ab} and directional PSP-coupled emission at λ_{em}. The employing of diffraction gratings for plasmon-enhanced fluorescence assays as an alternative to the more often used Kretschmann configuration of attenuated total reflection method [3, 8] was explored in the past by using rectangular one-dimensional [13] and a two-dimensional [14] Ag gratings with a SiO_2 protection layer. These structures showed an enhancement factor up to $EF = 10^2$ when compared to flat glass substrate. When applied to an assay, this approach was demonstrated to improve the LOD by a factor of 26 [15]. The presented work reports a complete model for optimization of plasmonic amplification of fluorescence on relief diffraction gratings that takes into account combined PSP-driven excitation and emission from randomly oriented emitters. Based on the finite difference time domain (FDTD) simulations,

crossed gratings are designed, prepared, and their performance characterized in terms of enhancement factor. Finally, the gratings are employed for signal amplification in fluorescence-based immunoassay for detection of interleukin 6 (IL6) biomarker. In particular, the plasmonic substrates are designed to assure compatibility with established fluorescence readers that rely on epi-fluorescence geometry. Devices with such detection geometry including various microscopes and fluorescence scanners are routinely used in microbiology laboratories for e.g., readout of assays with microarray detection format.

2. Investigated geometry

The presented study concerns amplification of fluorescence sandwich immunoassays by the near field coupling of organic dye labels with PSP modes supported by crossed relief Au grating, see Fig. 1(a). The Au surface is periodically corrugated in order to excite PSPs by a normally incident laser beam by first order diffraction. The wavelength of the excitation beam of λ_{ex} = 633 nm is chosen in order to overlap with the absorption band of used Alexa Fluor 647 dye that exhibits an intrinsic quantum yield of η_0 = 0.33. The surface plasmon-coupled emission is converted to the far field by diffraction on the same grating at the emission wavelength of Alexa Fluor 647 dye of λ_{em} = 670 nm.

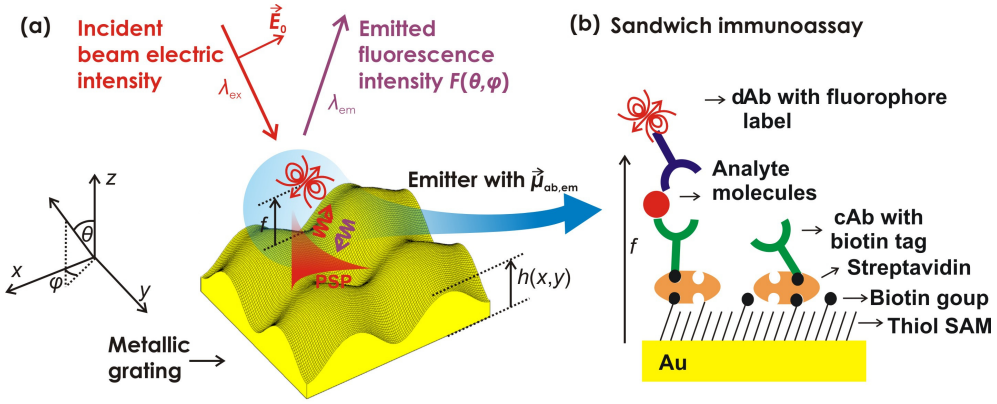

Fig. 1. (a) Schematic of the investigated geometry where an emitter with defined absorption and emission dipole moments $\mu_{ab,em}$ is placed above a crossed gold grating at a distance f. The emitter represents a fluorophore label attached to a detection antibody (dAb) that is used in (b) sandwich immunoassay.

The grating profile is optimized to simultaneously provide strong coupling of the excitation beam to PSPs and to re-emit the fluorescence power carried by PSPs perpendicular to the surface into an acceptance numerical aperture of NA = 0.2. The corrugation profile of the grating surface was described by using Cartesian coordinates (x and y defined in Fig. 1(a) as the function $h(x,y) = \alpha(\sin[(2\pi/\Lambda)x] + \sin[(2\pi/\Lambda)y]) + \beta(\sin[(2\pi/\Lambda)x] + \sin[(2\pi/\Lambda)y])^2$, where Λ is the period and α and β are modulation amplitudes. The parameters of the crossed grating profile used further are Λ = 434 nm, α = 4 nm and β = 2.5 nm. When applied for sandwich immunoassay, the Au grating is modified with a thiol self-assembled monolayer (SAM) and streptavidin that serves as a linker for attaching a capture antibody [cAb with biotin tags is shown as a green molecule in Fig. 1(b)]. The cAb affinity binds the target analyte present in an aqueous sample [see red molecule in Fig. 1(b)] and is detected by using an additional detection antibody [dAb depicted as a blue molecule in Fig. 1(b)] that carries a fluorophore label. Taking into account the thickness of thiol SAM of 3 nm, the size of the immunoglobulin G antibody of around 8 nm [16] and the size of streptavidin of around 4 nm [17], the distance between the gold surface and fluorophore label that serves as a reporter of the target molecule affinity binding events was estimated between f = 15 and 20 nm.

3. Materials and methods

3.1. Materials

Positive photoresist Microposit S1805 was purchased from Shipley and its developer AZ 303 was acquired from MicroChemicals. Polydimethylsiloxane elastomer (PDMS) Sylgard 184 was obtained from Dow Corning and the UV-curable polymer Amonil MMS 10 was from AMO GmbH. The organic dye 1,1'-dioctadecyl-3,3,3′,3′-tetramethylindodicarbocyanine, 4 chlorobenzene-sulfonate salt (DiD) from Invitrogen was dissolved in toluene and blended with poly(methyl methacrylate) (PMMA) from Sigma-Aldrich. Biotinylated PEG alkane thiol ($C_{33}H_{63}N_3O_8S_2$, molecular weight of 694 Da) was purchased from SensoPath Technologies and triethylene glycol mono-11-mercaptoundecyl ether ($C_{17}H_{36}O_4S$, molecular weight of 336.5 Da) was obtained from Sigma Aldrich. Streptavidin (SA, molecular weight of 52.8 kDa) was purchased from Carl Roth GmbH + Co. KG. The biotinylated capture antibody (c-Ab, anti-Human IL-6 Biotin) against human interleukin 6 was from eBioscience (product number 13-7068). Affinity-purified recombinant protein carrier-free human IL-6 was from eBioscience (product number 34-8069). As a detection antibody (dAb), affinity purified monoclonal anti-human IL-6 from eBioscience was used and labeled by the Alexa Fluor 647 Protein Labeling Kit (A20173) from Molecular Probes / Invitrogen. Samples were prepared in phosphate buffered saline (PBS) with 0.05% Tween 20 (from Sigma Aldrich)

3.2. Preparation of crossed relief gratings

The relief crossed grating structure was recorded by UV laser interference lithography (LIL) with Lloyd's mirror configuration into the photoresists, developed, and afterwards copied by UV nanoimprint lithography (UV-NIL) similar to our previous works [18, 19]. Firstly, a photoresist Microposit S1805 layer was deposited on a cleaned BK7 glass substrate by spin-coating at 5000 rpm for 45 s followed by soft baking on a hot plate at 95°C for 2 min. Afterwards, the sample was mounted to the LIL setup. The angle of interfering expanded beams (with intensity of 15.7 μW/cm^2) emitted from a HeCd laser (model IK 3031 R-C from Kimmon) at wavelength λ = 325 nm was set to 21.97 deg which corresponds to a period of Λ = 434 nm. The photoresist layer on the BK7 glass substrate was exposed to the interference field for 120 s. Then the substrate was rotated by 90 deg and exposed again to the interference field under the same conditions. After the exposition, the relief corrugation was etched to the resist by the developer AZ 303 that was mixed with distilled water at the ratio of 1:14 for t_{dev} = 80 s. This structure was used as a master for further replication by UV-NIL. Firstly, the photoresist relief grating was casted to PDMS that was cured at room temperature for 3 days. The PDMS copy was detached from the master and employed as a working stamp. UV-curable polymer Amonil MMS 10 was spin-coated on a cleaned BK7 glass substrate at 3000 rpm for 120 s which results to a layer with a thickness of 110 ± 7 nm. Then, the PDMS working stamp was placed on the top of the Amonil surface and irradiated by UV light (UV lamp Bio-Link 365, Vilber Lourmat) at λ = 365 nm. The irradiation dose was 10 J/cm^2. Finally, the PDMS stamp was detached from the cured Amonil MMS 10 leaving a copy of the master structure. The copied gratings were subsequently coated with 4 nm of Cr and 100 nm of Au by vacuum thermal evaporation (HHV AUTO 306 from HHV LTD) in vacuum better than 10^{-6} mBar. Let us note that each grating sample comprised an area that was structured and an area that was flat and served as a reference in the further optical measurements

3.3. Surface modifications

For angularly-resolved fluorescence measurements, prepared samples with a measuring pad (where the Au surface is structured) and reference pad (where the Au surface is flat) were coated by a thin PMMA layer with dispersed organic dye (DiD). The DiD dye was dissolved in toluene and blended with PMMA at a concentration of 60 μM and 0.25 wt%, respectively. This mixture was spin-coated on the Au surface at 3000 rpm for 60 s and dried for 60 min.

The layer was intentionally kept thin (a thickness of around 6 nm was measured by surface plasmon resonance - SPR) in order to approximate the surface mass density of protein biointerface that was used in subsequent immunoassay experiments.

For immunoassay experiments, a freshly prepared Au film was incubated in an ethanol solution with dissolved thiols carrying functional biotin (biotinylated PEG alkane thiol) and passivating PEG (triethylene glycol mono-11-mercaptoundecyl ether) groups. The total thiol concentration was 1 mM and the molar ratio of functional (biotin) and passivating (PEG) thiols was 1:4. After overnight self-assembly of thiol monolayer (SAM), the samples were removed from the thiol solution, their surface was extensively rinsed with ethanol, and dried in a stream of air. Then, a flow-cell was attached to the sensor surface and the SA and cAb with biotin tags were subsequently affinity immobilized *in situ*. Each protein was dissolved in phosphate buffered saline (PBS) at the concentration of 50 μg/mL for the streptavidin and 5 μg/mL for the biotinylated capture antibody and flowed over the surface at the flow rate of 15 μL/min.

3.4. Optical setups

Two optical configurations have been used for the fluorescence immunoassay measurements and for the characterizing the angular distribution of the fluorescence light emitted from plasmonic substrates, see Fig. 2. A beam emitted from a He-Ne laser (power of about 2 mW) at λ_{ex} = 632.8 nm subsequently passed through a laser band-pass filter (FL632.8-10 from Thorlabs), a polarizer, and a neutral density filter (1%). Afterwards the laser beam was reflected by a dichroic mirror (XF2087 660DRLP from Omega Optical) towards the substrate with corrugated or flat Au areas. The dichroic mirror was tilted by 45 deg where it is highly reflective at the wavelength λ_{ex} and transparent at the emission wavelength of λ_{em} = 670 nm. Against the Au surface a flow-cell was clamped in order to contain aqueous samples. A flow cell with a volume of 1.5 μL was made from a thin PDMS gasket and a transparent fused silica glass substrate. Into the silica substrate, inlet and outlet ports were drilled and connected by tubing (Tygon R3607, 0.13 mm) to a peristaltic pump. For the experiments with DiD dye, a drop of water was placed to the surface of the plasmon substrate and covered with a thin microscope cover glass.

The intensity of fluorescence light emitted from the Alexa Fluor 647 was measured in time by a system that is similar to that used in epi-fluorescence microscopy, see Fig. 2(a). The fluorescence light emitted from the sensor surface passed through the dichroic mirror and was collected by a lens (focal length f = 50 mm and numerical aperture of NA = 0.2, LB1471 from Thorlabs). Before the lens, the fluorescence beam travelled through a spatial filter that blocked the partially reflected excitation beam at the wavelength λ_{ex} (blocking the light emitted to cone with polar angle θ<1 deg). As the sample surface was placed to the focal plane of the collection lens, the fluorescence beam was collimated and passed through a set of filters. The set of filters consisted of a notch filter (XNF-632.8-25.0M from CVI Melles Griot) that was used to block the excitation wavelength λ_{ex} and two bandpass filters (FB670-10 from Thorlabs and 670FS10-25 from Andover Corporation Optical Filter) with the transmission window centered at the λ = 670 nm and spectral width of about 10 nm. Finally, the fluorescence beam was focused at the input of a photomultiplier (H6240-01, Hamamatsu) that was connected to a counter (53131A from Agilent). The output from the counter was recorded in counts per second (cps) by using software Wasplas developed at Max Planck Institute for Polymer Research in Mainz (Germany).

The fluorescence light emitted from DiD dye was collected by using microscope objective lens (36-133 with numerical aperture of NA = 0.65 and working distance WD = 0.52 mm from Edmund Optics). The sample was positioned to the focal plane of the lens and thus the collected fluorescence light was collimated and travelled through a dichroic mirror and a set of filters identical to those used in previous system, see Fig. 2(b). The spatial distribution of fluorescence light intensity was measured by a CCD camera (EM-CCD iXon + 885 from

Andor Technology) that was cooled by a Peltier element to −50 °C to reduce the pixel noise. All acquired images were background compensated and accumulated over 20 s in order to improve the signal-to-noise ratio. The spatial distribution was converted to angular distribution based on the knowledge of the focal length of used lens and the polar θ and azimuthal φ angles were used as defined in Fig. 1(a).

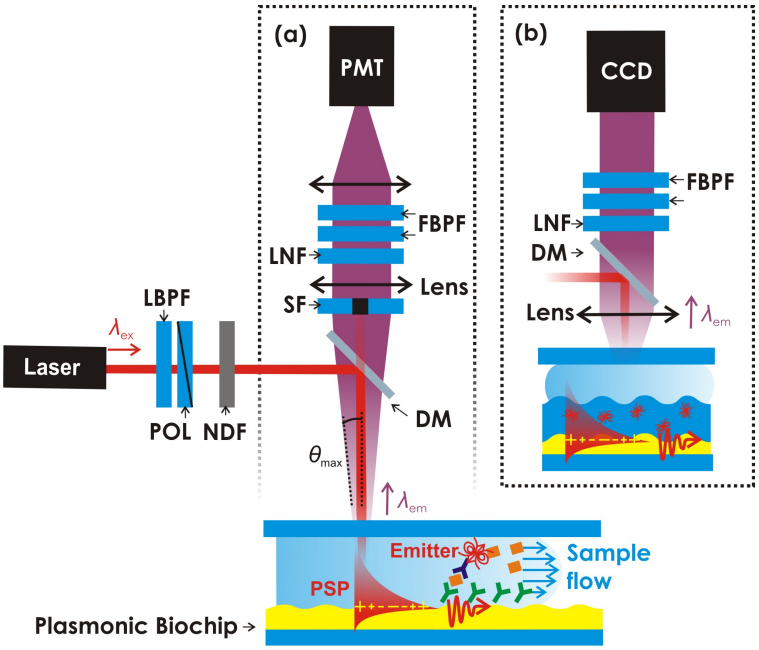

Fig. 2. Schematic optical setups for the excitation and collecting of fluorescence light emitted from a plasmonic sensor chip. A laser band-pass filter (LBF), polarizer (POL), neutral density filter (NDF), dichroic mirror (DM), spatial filter (SF), laser notch filter (LNF), and fluorescence band-pass filter (FBPF) were used. Section (a) was used for immunoassay fluorescence measurement and (b) for the angular resolved fluorescence measurement.

3.5. Simulation parameters

The finite difference time domain (FDTD) method was used for the simulation of the grating-coupled SPR reflectivity spectra, near field distribution of the electric intensity, and far-field emission from an emitter similar to our previous study [20]. The refractive index of gold n_m was obtained from literature [21] and the refractive index of water set to n_b = 1.33 (the dependence on wavelength was omitted). Electrical field intensity at λ_{ex} was normalized with that of incident beam $|E/E_0|^2$ and reflectivity spectra $R(\lambda,\theta)$ were calculated with a single unit cell and periodic boundary conditions applied in x and y direction. A perfect metallic conductor was placed below the structure with optically thick Au film (thickness of 300 nm). A perfectly matched layer (PML) was placed above the structure at the distance of z = 1500 nm from the metal surface. A uniform mesh of 1 nm was chosen for the simulation region.

Simulations of the far-field emission of a fluorophore at the wavelength λ_{em} in the vicinity to the plasmonic substrate were carried by representing a fluorophore as a dipole current source. The simulation cell with the length of 46 periods in x and y directions was chosen in order to achieve convergence (let us note that the length of simulation cell of about 20 μm is much larger than the propagation length of PSP on Au at λ_{em}). Four PMLs were placed at vertical boundaries of the cell (plus and minus, x and y directions). A perfect electric conductor was used as boundary condition below the optically thick gold grating (minus z direction). In the z direction above the structure PML was used. The central part of the

structure with the lateral size of one period (in both x and y directions) where a dipole was placed was modeled with a maximum mesh size of 2.5 nm, while the rest of the structure was modeled with a maximum mesh size of 5 nm. The simulated enhancement factor of fluorescence intensity EF was averaged over all orientations of the dipole and it took into account random position on the surface at a chosen distance f from the Au surface:

$$EF = \frac{\left\langle \left| \vec{E}(\lambda_{ex}) \cdot \vec{\mu}_{ab} \right|^2 \times \eta \times CE \right\rangle}{\left\langle \left| \vec{E}_0(\lambda_{ex}) \cdot \vec{\mu}_{ab} \right|^2 \times \eta_0 \times CE_0 \right\rangle}, \quad (1)$$

where brackets denote the averaging over the orientation and location of the absorption dipole $\vec{\mu}_{ab}$, $\vec{E}$ is the electric field vector above the metallic surface and $\vec{E}_0$ is the electric field of incident plane wave. η states for the quantum yield of the emitter that is changed from that in a bulk solution η_0 due to the presence of the metallic surface. The quantum yield was calculated from the modified total and radiative decay rates as reported previously [20, 22]. Briefly, the energy flux from a randomly oriented dipole in bulk solution without the metallic structure and when placed above the metallic grating structure (comprising the 46 periods in x and y directions and the dipole) was calculated. The changes in quantum yield were determined from obtained total emitted power (by using energy flux detector closely surrounding the dipole), power emitted to the far field (by using energy flux detector surrounding the complete structure) and from the knowledge of the intrinsic quantum yield of the emitter in water η_0. The CE describes the collection efficiency of the fluorescence light intensity F obtained as:

$$CE = \int_0^{2\pi} \int_0^{\theta_{max}} F(\theta, \varphi, \vec{\mu}_{em}) \sin\theta d\varphi d\theta \Big/ \int_0^{2\pi} \int_0^{\pi} F(\theta, \varphi, \vec{\mu}_{em}) \sin\theta d\varphi d\theta, \quad (2)$$

where θ_{max} = 11.5 deg is the maximum acceptance polar angle. CE_0 is the collection efficiency from a randomly oriented emitter present in water without the metallic surface.

4. Results and discussion

5.1 Simulations

As Eq. (1) illustrates, the fluorescence intensity enhancement due to the near field coupling of the emitter with PSPs on structured surface can be obtained as a product of enhanced excitation rate, increased collection efficiency CE by the directional surface plasmon-coupled emission, and changed quantum yield η/η_0. For the excitation far from saturation, the excitation rate is proportional to the strength of the electric field intensity at the excitation wavelength λ_{ex}. Simulations in Fig. 3(a) show the coupling of normally incident plane wave at λ_{ex} to PSPs via diffraction orders (0, ± 1) and (± 1,0) which leads to the enhancement of electric field intensity of $|E/E_0|^2$ = 46 and 44 at the distance from the metal surface f = 15 and 20 nm, respectively. Let us note that these data were obtained by averaging the field profile over the unit cell [see an example of the cross-section of the near field electric intensity distribution in Fig. 3(b)]. The averaged values of PSP-amplified electric field intensity are about 41 (for f = 15 nm) and 32 (for f = 20 nm) times larger than those simulated for a flat Au surface ($|E/E_0|^2$ = 1.12 and 1.36 for f = 15 and 20 nm, respectively).

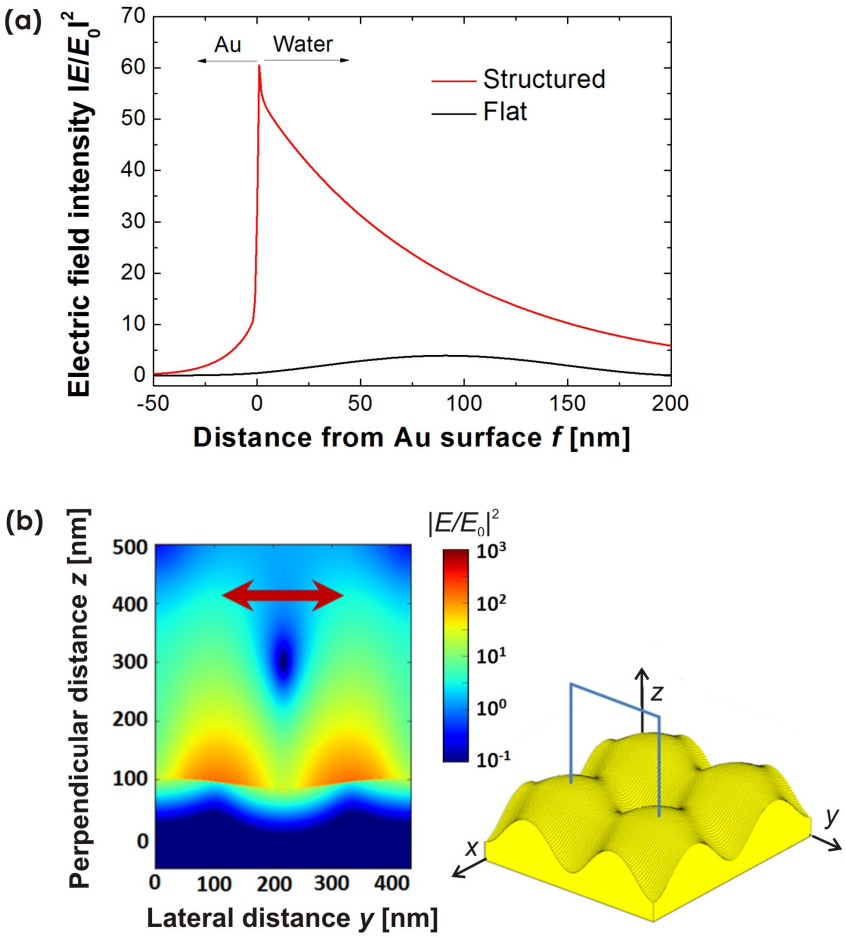

Fig. 3. (a) Electric field intensity $|E/E_0|^2$ averaged over the unit cell. The field strength was calculated as a function of distance f from the flat and corrugated gold surface f for normally incident plane wave at the wavelength of λ_{ex} = 633 nm and the polarization of electric intensity vector E_0 parallel to y axis. (b) Example of the near field electric intensity for indicated cross-section of the unit cell and polarization of the excitation beam noted as an arrow.

After the excitation, the emitter radiates light at the wavelength λ_{em} directly to the far field, via PSP modes, or becomes quenched due to Förster energy transfer. A randomly oriented dipole above flat Au surface emits the maximum portion of power via PSPs (65%) at the distance of f = 18 nm [9]. At this distance, a smaller fraction of energy is emitted directly to the far field (25%) and becomes quenched (10%). The periodic corrugation of the surface allows retrieving the energy emitted via PSPs (which is otherwise trapped and dissipated due to Ohmic losses in the metal) by its re-emission into the far field where it can contribute to the detected fluorescence signal. Figure 4(a) presents simulated angular distribution of fluorescence intensity $F(\theta,\varphi)$ emitted at a distance of f = 20 nm from above the flat (left) and corrugated (right) surfaces. These data show that on the flat surface, the emission is rather isotropical while on the structured surface, four bright characteristic bands occur due to the diffraction out-coupled PSPs by diffraction orders m = (± 1,0) and m = (0, ± 1). Let us note that the emissions from the distance of f = 15 nm and 20 nm shows identical features in the angular distribution $F(\theta,\varphi)$ and only the overall intensity differs. A cross-section of the emission shown in Fig. 4(b) illustrates that the emitted intensity from corrugated surface via

PSPs occurs preferably in a narrow cone at polar angles $\theta<\theta_{max}$ = 11.5 that correspond to *NA* = 0.2 for the assumed epi-fluorescence geometry.

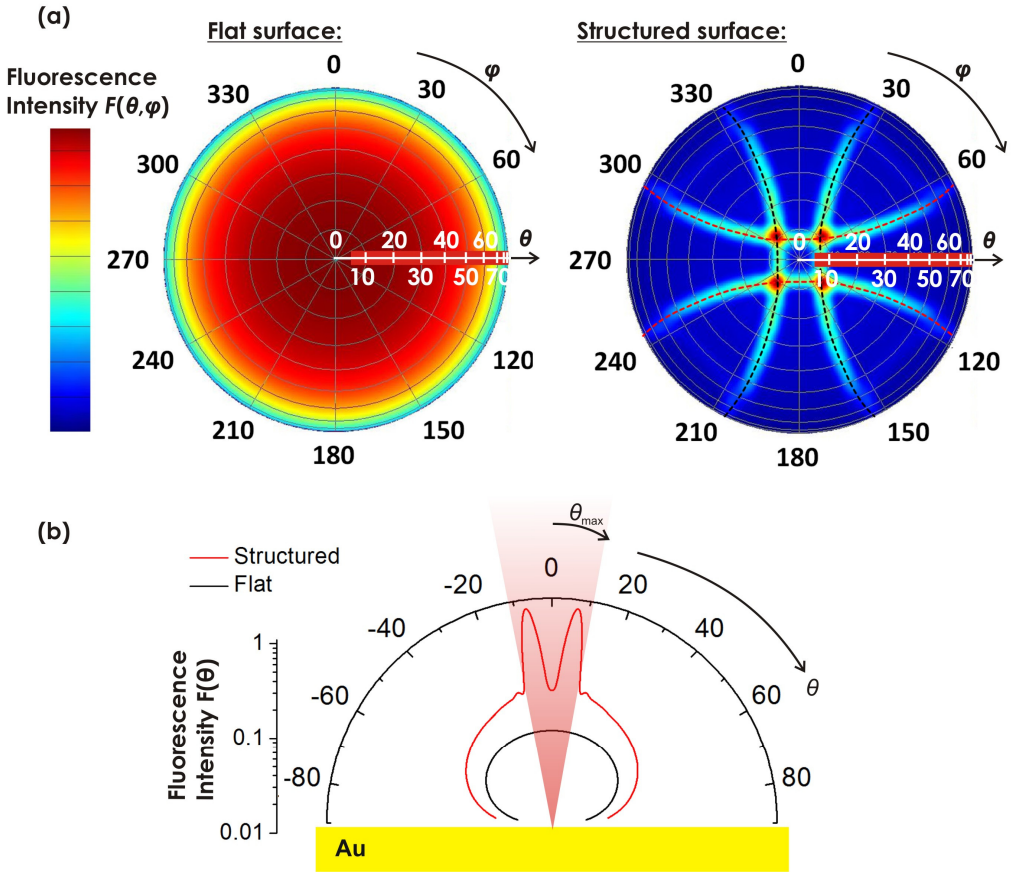

Fig. 4. (a) Simulations of angular distribution of far-field fluorescence intensity $F(\theta,\varphi)$ from randomly oriented fluorophore that emits at a distance f = 20 nm from a flat (left) and corrugated (right) gold surface at a wavelength of λ_{em} = 670 nm. Both distributions are normalized to the maximum intensity. (b) For the same geometry, a comparison of far-field fluorescence intensity $F(\theta)$ from above the flat and corrugated surfaces was calculated for the azimuthal angle $\varphi = 0$. The polar angle θ is assumed in air and the refraction at the interfaces is taken into account.

Table 1 presented below shows that the proximity to the metal surface decreases the quantum yield of the assumed dye (Alexa Fluor 647 with intrinsic quantum yield of $\eta_0 = 0.33$) at the distance of f = 15 and 20 nm to $\eta = 0.22$ and $\eta = 0.28$, respectively. However, this loss is compensated by the effect of enhanced excitation rate and directional fluorescence emission perpendicular to the surface. Table 1 summarizes the simulated enhancement of emitted fluorescence intensity on corrugated and flat gold surfaces as well as the key contributions of the increased excitation rate (proportional to enhanced field strength $|E/E_0|^2$ at λ_{ex}), decreased quantum yield η/η_0, and increased collection efficiency $<CE>$. These data predict the enhancement factor between EF = 145 at a distance of f = 15 nm and EF = 96 at the farther distance f = 20 nm.

Table 1. Summary of Key Contributions to EF (Defined as Ratio of Fluorescence Signal Emitted from Structured and Flat Surfaces) for Randomly Aligned Absorption and Emission Dipoles Placed at a Distance of f = 15 and 20 nm from an Au Surface

	Flat f = 15 nm	**Structured** f = 15 nm	**Flat** f = 20 nm	**Structured** f = 20 nm
$\lvert E/E_0\rvert^2$ at λ_{ex}	1.12	46.1	1.36	43.6
η/η_0	0.68	0.68	0.84	0.82
$<CE>$ at λ_{em}	1.3%	6.1%	1.4%	5.9%
EF(structured vs. flat)	145		96	

5.1 Experimental

In order to check the spectrum of PSP modes excited on the surface of prepared crossed Au grating that was brought in contact with water, reflectivity dependence on the wavelength λ and polar angle θ was measured for fixed azimuthal angle $\varphi = 0$. As Fig. 5(a) and Fig. 5(b) show, the diffraction coupling occurs close to the predicted wavelength at $\lambda = 631.5$ nm when the transverse magnetic (TM) or transverse electric (TE) polarized beam is normally incident to the surface. When increasing the polar angle θ, the SPR resonance splits to two branches due to coupling via plus and minus diffraction order (0, ± 1) in the TM polarization. At the emission wavelength $\lambda_{em} = 670$ nm, the resonance occurs at polar angle of $\theta = 8$ deg which is inside the acceptance range of polar angles of the used collection lens ($\theta<\theta_{max} = 11.5$ deg for the $NA = 0.2$). For the TE polarization the resonance depends weakly on the polar angle. In addition, Fig. 5(c) shows the measured profile of prepared grating. From the acquired morphology, the parameters of Λ, α, and β used in previous simulations were determined.

By using the optical system depicted in Fig. 2(b), the angular distribution of emitted fluorescence light $F(\theta,\varphi)$ from the structured and flat Au surfaces was measured. In this experiment a thin PMMA layer doped with DiD dye that exhibit similar fluorescence characteristics as Alexa Fluor 647 was deposited to the surface. The surface was brought in contact with water and excited by a normally incident laser beam at $\lambda_{ex} = 633$ nm. At the emission wavelength $\lambda_{em} = 670$ nm, the fluorescence distributions $F(\theta,\varphi)$ presented in Fig. 6 were measured for flat and structured surfaces. These data agree with simulations in Fig. 4 which reveal identical angular location of increased intensity originating from surface plasmon-coupled fluorescence. Compared to simulations, the angular width of the bands is broadened due to the fact that the surface plasmon-coupled fluorescence is highly wavelength sensitive and the fluorescence light is collected in a wavelength band width of about 10 nm. The presented data confirm that the designed corrugation of the Au surface allows extracting fluorescence light intensity emitted via PSPs and concentrate it to a cone that propagates perpendicular to the surface at polar angles below the θ_{max}. By integrating the intensity within this cone, it was determined that the overall intensity emitted per attached dye into the numerical aperture $NA = 0.2$ was increased by a factor $EF>10^2$.

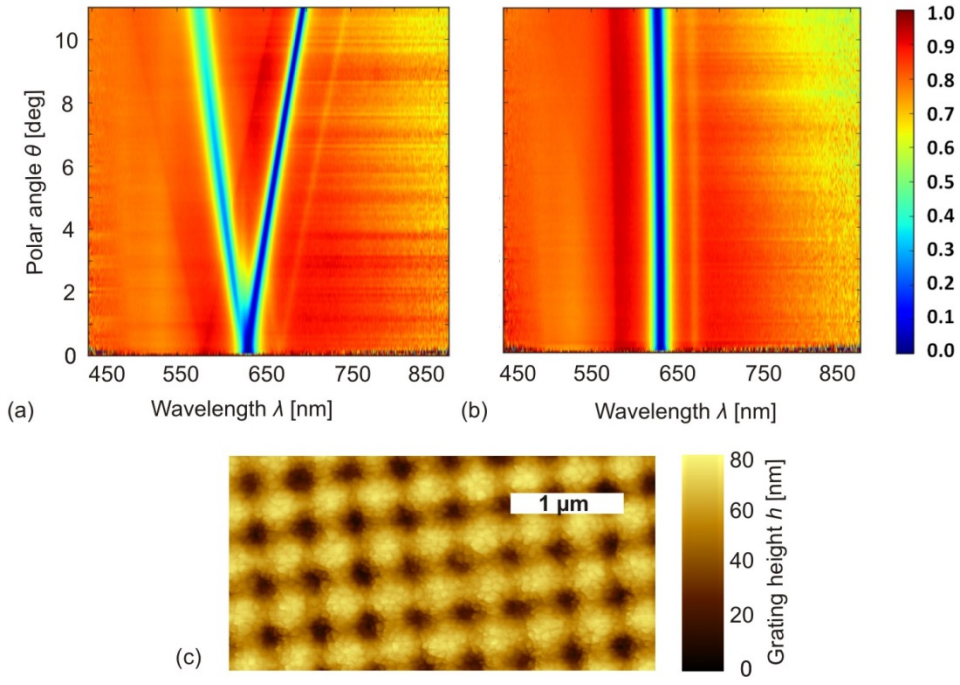

Fig. 5. Measured dependence of the reflectivity from corrugated gold surface on polar angle θ and wavelength λ. Azimuthal angle was set to $\varphi = 0$ and (a) TM and (b) TE polarization was selected for the excitation of PSPs at the interface between gold and water via diffraction orders (± 1,0) and (0, ± 1) respectively. (c) AFM characterization of the corrugated gold surface.

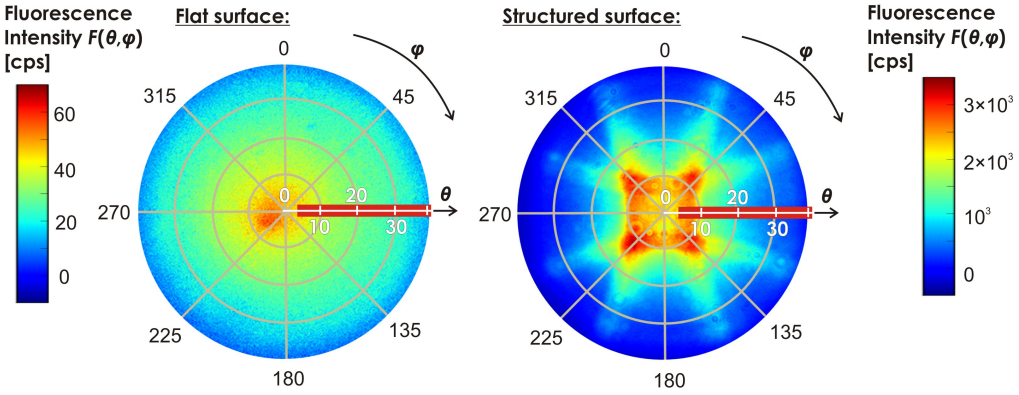

Fig. 6. Measured angular distribution of far-field fluorescence intensity $F(\theta,\varphi)$ emitted from randomly oriented DiD dyes dispersed in a PMMA layer that was attached to a flat (left) and corrugated (right) Au surfaces. The polar angle θ is given in air.

Finally, the prepared structures were tested for the amplification of fluorescence signal that is associated with the affinity binding of IL-6 by using the sandwich immunoassay format. The fluorescence intensity was measured in real-time with the optical system shown in Fig. 2(a). Figure 7(a) presents an example of the kinetics of fluorescence signal when samples with the IL-6 concentration of 0.43 and 4.3 nM were analyzed. Firstly, a buffer was flowed over the surface with immobilized cAb in order to establish a baseline. Afterwards, a solution with dAb dissolved at a concentration of 0.6 nM is introduced at time $t = 8$ min. As dAb molecules were labeled with Alexa Fluor 647 dye, the fluorescence signal increased by $\Delta F_B = 9.1 \times 10^3$ cps on structured surface due to the excitation of molecules present in the

bulk solution. After rinsing with PBS buffer at time t = 18 min, the fluorescence signal dropped down and the increase in the signal (difference before and after the flow of dAb) of $\Delta F = 2.2 \times 10^3$ cps was observed due to small unspecific sorption to the surface. After five minute rinsing with PBS, a sample with 0.43 nM concentration of IL-6 was flowed for 10 min followed by additional 9 min rinsing with PBS. Let us note that as IL-6 is not fluorescently active and thus no change in the signal F is observed. Then, the dAb dissolved at 0.6 nM concentration is injected to the sensor at time 42 min and affinity binds to IL-6 captured by cAb, see Fig. 1(b). This binding is associated with gradual increase in the fluorescence signal F. After the rinsing with PBST, an order of magnitude higher increase in the fluorescence signal of $\Delta F = 2.8 \times 10^4$ cps is observed due to the presence of IL-6 on the surface.

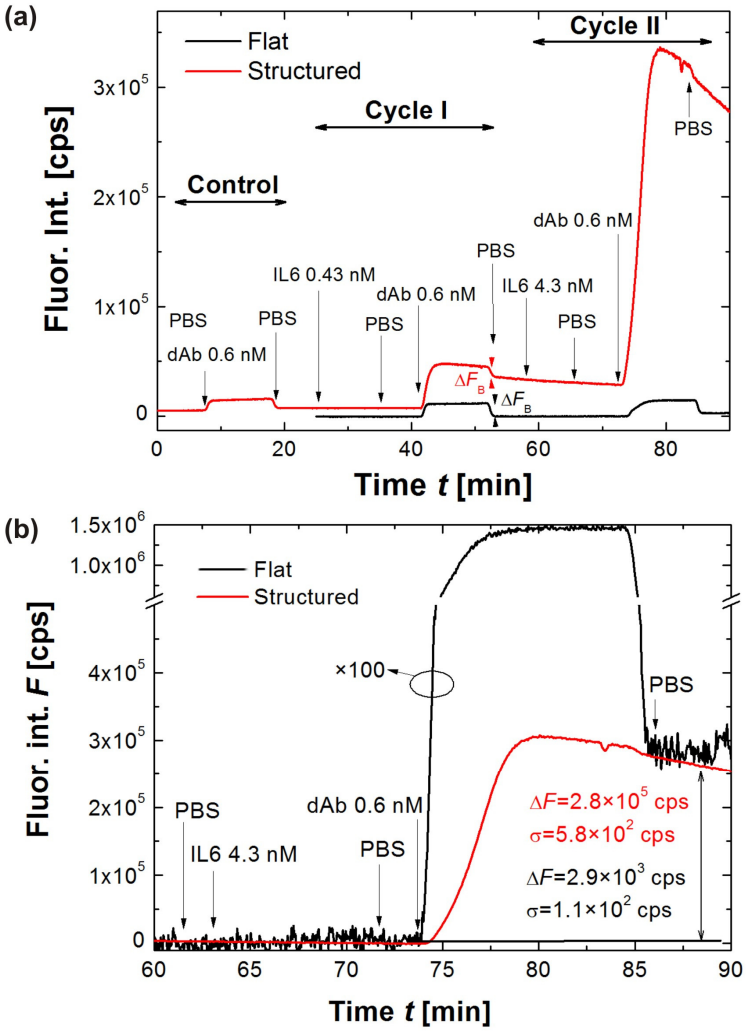

Fig. 7. (a) Kinetics of fluorescence intensity F measured upon a sandwich immunoassay with the IL-6 analyte concentration of 0 (control), 0.43 (cycle I), and 4.3 nM (cycle II). (b) Detailed comparison of the fluorescence intensity Fmeasured on structured and flat surface upon a sandwich immunoassay cycle with the analyte concentration of 4.3 nM.

An identical cycle was performed for 10-times higher IL-6 concentration of 4.3 nM (injection of dAb at time t = 74 min) which resulted in a fluorescence signal increase that was about an order of magnitude higher $\Delta F = 2.8 \times 10^5$ cps, indicating the sensor responds

linearly to the IL-6 concentrations. Figure 7(b) shows a detailed comparison of the fluorescence signal kinetics measured on structured (red curve) and flat (black) Au surfaces for the assay cycle with higher IL-6 concentration of 4.3 nM. It shows that the background signal due to the emission from labeled dAb in the bulk solution is slightly lower on the structured surface ($\Delta F_B = 9.1 \times 10^3$) than on the flat surface ($\Delta F_B = 1.2 \times 10^4$ cps) due to the fact that the reflection of the excitation beam is suppressed by its coupling to PSPs. However, the signal due to the affinity capture of target molecules on the corrugated surface is increased by the factor of $EF = 96$ which is close to the simulated enhancement factors for the distance between the metal and the emitter of $f = 20$ nm (see Table 1). The reason for this strong amplification is that the probing the reaction on the surface by confined field of PSPs selectively increases the fluorescence signal emitted from the surface and does not contribute to the background. This plasmonic amplification increases the signal-to-noise-ratio of the fluorescence signal ΔF associated to the binding of IL-6 at the concentration of 4.3 nM by a factor of 19 ($SNR = \sigma/\Delta F$). This value is better than the square root of the enhancement factor of EF which indicates that the statistics of noise for acquired fluorescence signal is not purely associated with a shot noise, but probably also contains additional (additive) noise of the readout electronics.

6. Conclusions

In summary, we present simulations and experiments demonstrating that the combination of enhanced excitation rate and directional emission originating from the coupling of emitters with the confined field of surface plasmons allows for amplifying measured fluorescence signal by a factor of $EF \sim 10^2$. This phenomenon was implemented by using a crossed relief diffraction grating to probe immunoassays for detection of molecular analytes with epi-fluorescence readout geometry that is similar to that used in regular fluorescence micro-array scanners or microscopes. The presented data confirm that the plasmonic amplification of fluorescence intensity translates to increased signal that is associated with affinity binding of target molecule – interleukin 6 – for a sandwich assay detection format and that the enhancement factor agrees with simulations and a model experiment with dyes dispersed in a polymer layer. The signal-to-noise ratio of signal acquired upon the immunoassay experiment was improved by a factor of 19. In addition, as the plasmonic amplification is highly surface selective it does not lead to an increase of background signal and allows observing molecular binding kinetics which are otherwise masked by the signal originating from labeled molecules dispersed in an aqueous sample flowed over the sensor surface. This feature may provide a valuable extension of performance of fluorescence readers in microbiological or clinical laboratories that typically measure only endpoint fluorescence signal and are blind upon the time when surface reactions proceed.

Acknowledgments

This work was partially supported by the Austrian NANO Initiative (FFG and BMVIT) through the NILPlasmonics project within the NILAustria cluster (www.NILAustria.at), Austrian Science Fund (FWF) through the project ACTIPLAS (P244920-N20) and FEMTECH – Frauen in Forschung und Technologie Initiative of the Austrian Ministry for Transportation, Innovation and Technology.